3D-Printed SiC Cold Plate with Evaporator Wicks

Mohammad Reza Shaeri*, Maksym Demydovych

Advanced Cooling Technologies, Inc., Lancaster, PA 17601, USA
*Corresponding author: MohammadReza.Shaeri@1-act.com

***Abstract*—In this study, a two-phase silicon carbide (SiC) ceramic cold plate, incorporating evaporator wicks for the thermal management of high-heat-flux electronics, was 3D printed. The cold plate featured two heaters, one located on the top and the other on the bottom, with each heater assigned to a separate evaporator wick positioned on the opposite side. The cold plate was tested using the refrigerant R245fa as the working fluid, and its performance was compared to two baseline cold plates of identical dimensions: a 3D-printed plain SiC cold plate (without evaporator wicks) and a 3D-printed aluminum alloy (AlSi10Mg) cold plate. Due to its high thermal conductivity, the aluminum cold plate operated above 526 W/cm^2 and achieved a highly uniform thermal resistance as low as 0.08 K-cm^2/W. Because of the lower thermal conductivity of SiC compared to aluminum, the plain SiC cold plate operated at lower heat fluxes and exhibited greater non-uniformity in thermal resistance across the cold plate. However, the performance of the wicked SiC cold plate was significantly enhanced due to the increased number of menisci, and the capillary pressure generated by the wicks. The wicked SiC cold plate operated above 445 W/cm^2 without any signs of partial dryout and achieved excellent uniformity in thermal resistance, as low as 0.12 K-cm^2/W, while operating with a low pumping power below 0.1 W. The fact that the thermal performance of the wicked SiC cold plate is comparable to that of a highly thermally conductive metal cold plate makes the wicked SiC cold plate an attractive thermal management solution for high-heat-flux power electronics applications that require ceramic cold plates, particularly those made of SiC. Additionally, the streamlined 3D printing process for fabricating wicked SiC cold plates enables the commercialization of this technology for power electronics.**

Keywords— SiC ceramic cold plate; Evaporator wick; CTE-match cold plate; Two-phase heat transfer; Additive manufacturing.

I. INTRODUCTION

As a key component of electronic packaging, a thermal management solution plays a crucial role to maintain the temperature of electronic devices below their maximum allowed operating temperature, thereby increasing their lifespan and reliability [1–3]. However, the rapid miniaturization of electronic components corresponds to intensely high heat flux and local hot spots, continuously posing challenges to the thermal management of these high-heat-flux devices [4,5]. Power electronics play important role in broad industrial sectors such as electrical power transmission, energy storage systems, transportation systems, custom power devices, etc. [6,7]. Power modules are comprised of multiple components made from different materials, each with its own coefficient of thermal expansion (CTE). One of the primary failure mechanisms in power electronic packaging is thermal stress, which arises from the mismatch in CTE of materials, with higher junction temperatures leading to increased stress and faster failure [8]. As a result, electronic packaging materials should ideally possess a low CTE and high thermal conductivity, alongside maintaining strong mechanical properties [9,10]. In a typical power electronics module, a semiconductor chip or die is placed onto a substrate, commonly a Direct Bonded Copper (DBC) substrate comprising a ceramic material, such as Aluminum Nitride (AlN), sandwiched between two copper layers. Subsequently, the substrate is mounted either onto a baseplate or directly onto a cold plate (i.e., a heat exchanger) using another bonded interface material [11–13].

Dissipating a large amount of concentrated heat from an electronic device exceeds the capabilities of air-cooled systems due to the poor thermal properties of air, as well as those of single-phase liquid cooling due to their requirement for large pumping power [14]. To address these issues, attention have been shifted towards phase-change cooling techniques that capitalize both sensible and latent heat of the working fluid [15]. Two-phase cold plates used for electronics cooling, such as micro/minichannel heat sinks and vapor chambers, have typically been fabricated using highly thermally conductive materials like copper and aluminum. To couple electronic chips to the cold plate surface, thermal interface materials (TIMs) are used to accommodate the CTE mismatch between the chips and the cold plate. However, as device heat flux increases, most current TIMs become less effective due to their relatively low thermal conductivity. While metallurgical bonds offer superior thermal resistance, the significant differences in CTE often lead to thermally induced fatigue failure of the joint [16,17]. A thermally superior design would allow the chip to be directly metallurgically bonded to the cold plate surface, requiring the cold plate material to have a CTE matched to typical chip materials, falling within the 3 to 6 ppm/°C range [16,17]. There are several related works, including the use of two-phase cold plates made of DBC AlN substrates [16–18]. AlN is characterized by its exceptional properties, including high thermal conductivity ~150 to 200 W/m.K, excellent stability at high temperatures, and a low CTE of ~ 4.5 ppm/°C [18]. The thin copper layers enable the use of conventional sintered wick structures and envelope sealing techniques, as well as direct circuit etching onto the surface of the cold plate [16]. Dussinger et al. [16] developed a low-CTE vapor chamber for thermal management of high-heat-flux microelectronic chips utilizing AlN ceramic with DBC layer as the envelope material. They removed over 700 W/cm^2 from a 1 cm^2 heat source area, achieving a measured evaporator thermal resistance ranging

between 0.05 to 0.1 K-cm^2/W. In a similar works, Ju et al. [17] developed a low-CTE vapor chamber made of DBC AlN, demonstrating the removal of over 1500 W with a heat input size of 4 cm^2, and achieving an evaporator thermal resistance as low as 0.075 K-cm^2/W. Shaeri et al. [18] fabricated a low-CTE two-phase minichannel heat sink using DBC AlN and demonstrated the removal of over 180 W/cm^2, with measured thermal resistances ~ 0.32 K-cm^2/W. In the works referenced in [16,17], the evaporators featured sintered wick structures developed on the copper layer of the DBC AlN plate. The porous wick structures enhance boiling and evaporation by increasing the number of nucleation sites and menisci, thus reducing thermal resistance. Moreover, the capillary pressure generated by wicks enhances the evaporator's ability to rewet, thereby increasing the upper limit of operation. However, the mismatch in CTE between ceramic and copper is the primary cause of substrate failure during thermal cycling tests, with over fifty percent of failures in DBC substrates attributed to delamination after forty cycles ranging from $-55℃$ to $+150℃$ [19,20]. Besides, the fabrication of complex-shaped ceramic pieces from AlN remains challenging due to their high hardness and brittleness. Conventional ceramic shaping methods, such as tape casting, injection molding, dry pressing, isostatic pressing, and gel casting, are inadequate for producing AlN ceramic components with intricate geometric shapes and interconnected channels [21]. Additionally, these methods necessitate the use of molds, which increases manufacturing expenses and consequently restricts the utility of AlN-based components [21,22].

Silicon carbide (SiC) ceramic exhibits excellent thermal conductivity, low density, excellent chemical stability, low CTE, high-temperature tolerance, high mechanical strength, wide band gap, etc., [23–25]. The outstanding properties of SiC have established it as an excellent material for fabricating heat exchangers, as detailed in previous research [23,26,27]. Due to the similar CTE of SiC to that of silicon, integrating the SiC cold plate closely with the chip enables the reduction of thermal resistance by eliminating several layers of substrates and TIMs between the chip and the cold plate.

In this study, a SiC cold plate, including evaporator wicks for the thermal management of high-heat-flux electronics, is fabricated through additive manufacturing (AM), and its performance is investigated across a wide range of heat fluxes. To demonstrate the performance of the wicked SiC cold plate, its thermal characteristics are compared with those of baseline cold plates, which are (i) a 3D-printed SiC cold plate without wicks, and (ii) a metal 3D-printed cold plate. Compared to traditional manufacturing techniques, AM, also known as 3D printing, reduces the multiple labor-intensive steps required for the fabrication of cold plates with complex features into a single or a few fabrication processes [28], which is a crucial step towards the commercialization of cold plates. This study is aligned with our ongoing research in the development of 3D-printed cold plates integrated with evaporator wicks [28–31].

II. Experiment

The schematic of the pumped two-phase loop is illustrated in Fig. 1. The loop consisted of a cold plate, several heat exchangers that operated as condensers, a reservoir, and a positive displacement pump. The heat rejected from the condensers was exchanged with lower-temperature water provided by a chiller. At various locations in the loop, T-type thermocouples, pressure transducers, and flowmeters were integrated. All components of the loop were interconnected by stainless steel tubes.

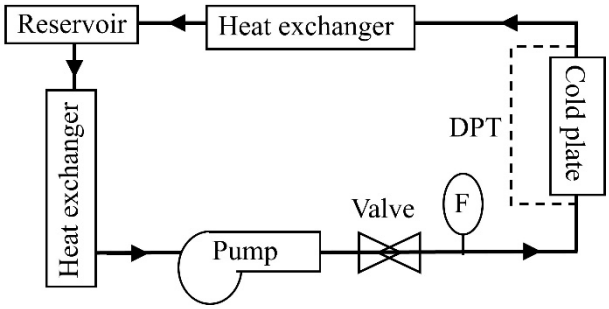

Fig. 1. Schematic of the pumped two-phase loop. F and DPT represent the flowmeter and differential pressure transducer, respectively.

Fig. 2 illustrates the CAD model of the cold plate, which includes one pedestal on each side of the cold plate. The pedestals were designed to position the heaters.

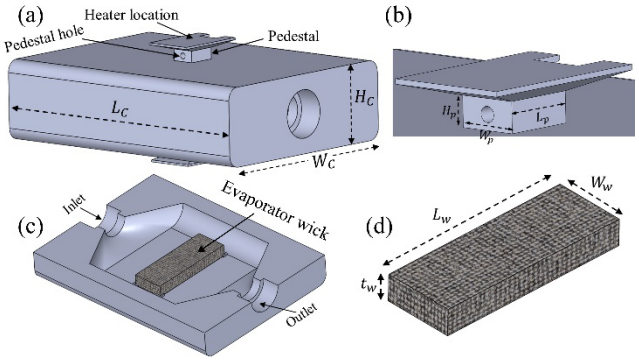

Fig. 2. CAD model of the (a) cold plate, (b) pedestal, (c) interior of the wicked SiC cold plate, (d) evaporator wick.

Initially, the cold plate was designed for thermal management of electronics with a footprint area identical to the small area of the pedestal, $L_p \times W_p$, as shown in Fig. 2(b). However, due to the unavailability of off-the-shelf high-power heaters with the same footprint size, converging pedestals were designed to locate the heaters on the larger area of the pedestal. On each pedestal, a resistive heater was soldered to apply electrical heat. Current and voltage to each individual heater were supplied using a variable transformer. A heater holder unit was designed to press the heaters into the pedestal, ensuring continuous contact between each heater and its corresponding pedestal. Fig. 3 illustrates the heater holder unit. Additionally, the heater holder unit was used to connect the inlet and outlet tubes to their corresponding manifolds using gaskets. Brazing a tube made from a material that matches the CTE of SiC is challenging and is an ongoing area of research in our group. Corresponding diameters for the inlet and outlet of the cold

plate are 6.4 mm. The hermeticity of cold plate was assessed using a helium mass spectrometer, revealing a measured leak rate lower than 9×10^{-10} std. cc/s [32,33].

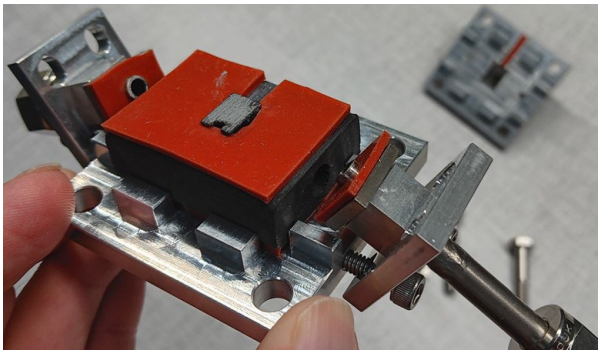

Fig. 3. The heater holder unit to connect the inlet and outlet tubes to the cold plate and to hold the heaters on the cold plate.

The cold plates and wicks were 3D printed through a process that uses a combination of binder jet printing and chemical vapor infiltration. The printing process creates a low density preform of the desired shape from SiC carbide powder. The preform is then densified by depositing high purity SiC, filling the internal porosity and sealing the surface. The process provides near net shape and high purity SiC components of complex geometry. The purity of SiC ceramic after final densification is greater than 99%.

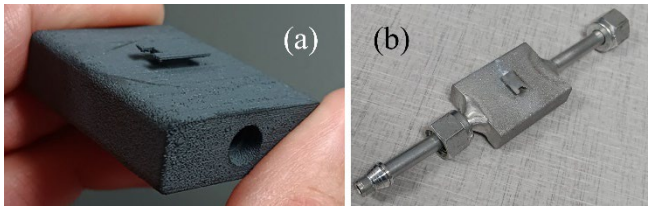

Fig. 4. Image showing: (a) the 3D-printed SiC cold plate, (b) the 3D-printed Al cold plate.

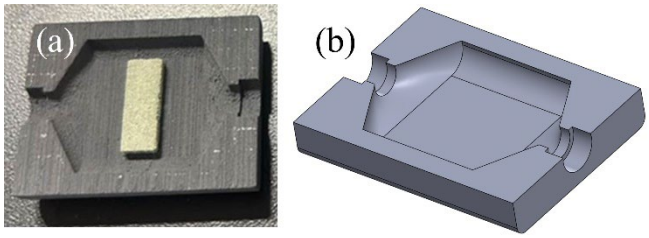

Fig. 5. (a) Image of the interior of the W-SiC cold plate with the evaporator wick, (b) the CAD model of the interior of the P-SiC cold plate.

As baselines for comparison, two additional cold plates with the same dimensions as the wicked SiC cold plate were fabricated using one single 3D printing process. One cold plate was made from AlSi10Mg and will be referred to as the aluminum cold plate. The other cold plate was made from SiC ceramic but without evaporator wicks; this will be referred to as the plain SiC cold plate. Throughout the rest of the paper, the wicked SiC cold plate, plain SiC cold plate, and aluminum cold plate will be designated as W-SiC, P-SiC, and Al cold plates, respectively. The 3D printing process for the P-SiC cold plate was similar to that used for the W-SiC cold plate. The Al cold plate was fabricated through Direct Metal Laser Sintering (DMLS) process. The 3D-printed SiC cold plate and Al cold plate are presented in Fig. 4. Additionally, Fig. 5 displays the interior of the W-SiC cold plate and the CAD model of the interior of the P-SiC cold plate. Geometrical information for the cold plates is described in Table 1. The corresponding dimensions described in Table 1 are schematically illustrated in Fig. 2.

TABLE 1. Geometrical information of the cold plate.

L_C, W_C, H_C	38.1 mm, 28.7 mm, 10.4 mm
L_w, W_w, t_w	15.2 mm, 5.6 mm, 2.0 mm
H_p, W_p, L_p	1.5 mm, 3.0 mm, 3.8 mm

The entire loop was checked to detect any leaks prior to charging the loop with the refrigerant R245fa. The pump speed and the control valve were adjusted to supply the cold plate with the desired flow rate of 1.0 LPM (liter per minute). The chiller temperature was set to keep the inlet temperature to the cold plate at 18.7 °C. Electrical heat input to each heater was increased by adjusting the voltage of the variable transformer. The outflow from the cold plate was directed to a heat exchanger, which acted as a condenser, and then directed to a liquid reservoir. Another heat exchanger, serving as a condenser, was placed after the reservoir and before the pump to ensure that the pump's inlet flow was a single-phase liquid. The subcooled liquid was then pumped into the cold plate, completing the loop. During steady-state conditions, signals from thermocouples, pressure transducers, flowmeters, and heaters were recorded by a data acquisition system. Steady-state conditions were determined when temperature variations remained minimal over an extended period of system operation.

The entire heater unit was covered with insulation layers to minimize heat dissipation to the surroundings. To calculate heat loss, single-phase cooling tests were conducted and the heat transfer ratio (ϕ), corresponding to the proportion of effective heat absorbed by the working fluid to the electrical heat input was calculated as follows:

$$\phi = \frac{\rho \dot{V} c_p (T_{out} - T_{in})}{\sum_{i=1}^{2} V_i \times I_i} \quad (1)$$

where V_i and I_i are the voltage and current applied to the i-th heater, respectively. ρ, $\dot{V}$, and c_p are the liquid density, volume flow rate, and specific heat, respectively. T_{in} and T_{out} are the fluid temperature at the inlet and outlet of the heat sink, respectively. Then, the heat flux to the i-th pedestal, i.e., q_i, was calculated as follows:

$$q_i = \phi \frac{V_i \times I_i}{L_p \times W_p} \quad (2)$$

where L_p and W_p are the length and width of the pedestal attached to the cold plate, as shown in Fig. 2(b). In this study, the thermal characteristic of the cold plate is described by the

specific thermal resistance of the i-th heater (R_i), calculated as follows:

$$R_i = \frac{T_{s,i} - \left(\frac{T_{in} + T_{out}}{2}\right)}{q_i} \quad (3)$$

where $T_{s,i}$ is the source temperature of the i-th heater, measured using a T-type thermocouple inserted into the hole of the i-th pedestal, as shown in Fig. 2(a). Also, T_{in} and T_{out} are the temperatures at the inlet and outlet of the cold plate, respectively.

The uncertainties of the T-type thermocouples, dimensions, and resistive heaters were ± 0.5 ℃, $\pm 2.54 \times 10^{-2}$ mm, and $\pm 5\%$ of the electrical resistance, respectively. Using propagation of uncertainty analysis, the uncertainty in thermal resistance was below 8.2%.

III. Results

The cold plates were tested in a horizontal orientation, with one heater positioned on the top surface and another on the bottom surface of each cold plate. Fig. 6 illustrates the thermal resistances of the different cold plates at various heat fluxes. Letters B and T in parentheses represent the bottom and top heaters, respectively, located on each cold plate.

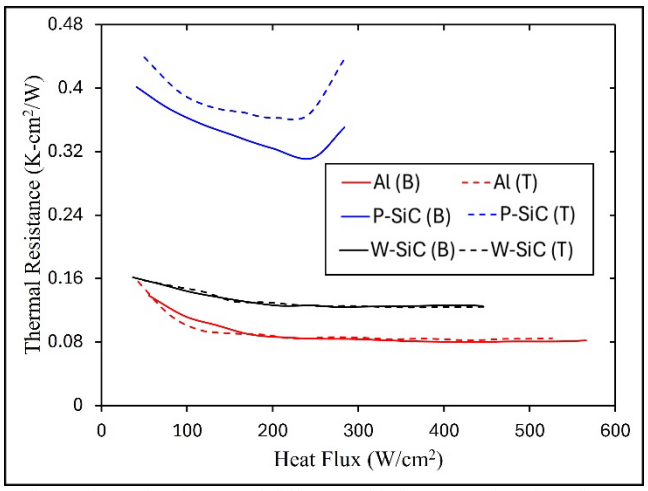

Fig. 6. Thermal resistance of different cold plates at various heat fluxes. Letters B and T in parentheses represent the bottom and top heaters, respectively, located on each cold plate.

An increase in heat load enhances evaporation/boiling, leading to a decrease in thermal resistance. This trend continues until reaching a global minimum thermal resistance associated with partial dryout. Partial dryout occurs when the rate of liquid depletion due to evaporation/boiling balances with the evaporator's rewetting capability [34]. Beyond this point, further increases in heat load result in a rise in thermal resistance, which accelerates the critical heat flux (CHF). In this study, CHF was identified by a sharp rise in the temperature of any of the heaters.

The Al cold plate operated at over 565 W/cm^2 for the bottom heater and 526 W/cm^2 for the top heater, without any signs of partial dryout. At this heat flux range, the cold plate achieved an excellent uniformity of thermal resistance as low as 0.08 K-cm^2/W. This low thermal resistance in the Al cold plate is attributed to the high thermal conductivity of aluminum. However, due to the lower thermal conductivity of SiC ceramic compared to aluminum, a lower performance is expected for the P-SiC cold plate. The P-SiC cold plate encountered partial dryout at heat fluxes around 245 W/cm^2, which essentially dictates the upper operational limit of the cold plate. The CHF occurred almost immediately in the P-SiC cold plate with a slight increase in heat load beyond partial dryout. Additionally, compared to the Al cold plate, the P-SiC cold plate showed a relatively wide gap in thermal resistance. In the heat flux range of ~ 245 W/cm^2, the measured thermal resistances of the P-SiC cold plate ranged from 0.31 to 0.37 K-cm^2/W for the bottom and top heaters, respectively.

However, implementing the evaporator wicks on the W-SiC cold plate substantially improved its thermal performance. The porous nature of wick structures in the W-SiC cold plate provided more nucleation sites for boiling and menisci for evaporation, leading to lower thermal resistance compared to the P-SiC cold plate. Additionally, the wicks generated capillary pressure, which improved the evaporator's rewetting capability; as a result, the W-SiC cold plate operated at a higher upper limit than the P-SiC cold plate. The thermal resistances of both heaters in the W-SiC cold plate continuously decreased as the heat load increased, without any indication of partial dryout. The upper operational limit for the heaters ranged from 445 to 450 W/cm^2, with excellent thermal resistance uniformity of ~ 0.12 K-cm^2/W. The fact that partial dryout did not occur in the Al and W-SiC cold plates indicates that these cold plates could potentially operate above their reported upper limits. However, to avoid excessively high source temperatures, the experiments were not extended beyond the maximum heat fluxes tested for each individual cold plate in this study.

Pumping power is a crucial factor in designing active thermal management solutions, as higher pumping power can limit the practicality of a cooling system, regardless of its thermal performance improvements [35]. Pumping power is calculated by multiplying the pressure drop across the system by the volume flow rate. In this study, the W-SiC cold plate operated within a low pumping power range, below 0.1 W.

The wicked SiC cold plate demonstrated a reasonably low thermal resistance and exhibited excellent uniformity of thermal resistance while operating at high heat fluxes without any signs of partial dryout, all while maintaining low pumping power. These merits position the cold plate as an attractive thermal management solution for applications that require ceramic cold plates for the thermal management of multiple high-heat-flux sources. Additionally, the use of additive manufacturing process for fabricating the entire cold plate significantly reduces production complexity and time compared to conventional manufacturing methods for similar cold plates. These important advantages represent crucial steps toward the commercialization of the wicked SiC cold plate developed in this study.

IV. Conclusion

A wicked SiC cold plate, fabricated through additive manufacturing, was tested using a pumped two-phase loop. The

cold plate featured two heaters located at the top and bottom. For comparison, two additional cold plates without evaporator wicks were 3D printed, one made from aluminum alloy and the other from SiC. Experiments were conducted across various heat fluxes, using R245fa as the working fluid. Although the Al cold plate demonstrated the best performance, the hydrothermal performance of the wicked SiC cold plate was also notable. The wicked SiC cold plate operated at heat fluxes above 445 W/cm^2, achieving thermal resistance of ~ 0.12 K-cm^2/W with excellent uniformity. Compared to the wicked SiC cold plate, the plain SiC cold plate exhibited lower thermal performances. The high thermal performance of the wicked SiC cold plate was achieved with pumping power below 0.1 W. Additionally, the full fabrication of the wicked SiC cold plate via 3D printing enhances the technology's potential for commercialization, making it attractive for thermal management of multiple high-heat-flux electronics.

ACKNOWLEDGMENT

Financial support by the Office of Science in the U.S. Department of Energy, award number DE-SC0018845 is gratefully acknowledged.

REFERENCES

[1] Mozafari, M., Lee, A., and Mohammadpour, J., "Thermal Management of Single and Multiple PCMs Based Heat Sinks for Electronics Cooling," *Thermal Science and Engineering Progress*, Vol. 23, 2021, p. 100919. https://doi.org/10.1016/j.tsep.2021.100919

[2] Singh, H., Mandel, R., Sarmiento, A., and Ohadi, M., "Thermal Management of High Flux Electronics Using Film Evaporation with an Enhanced Fluid Delivery System (FEEDS)," *International Communications in Heat and Mass Transfer*, Vol. 148, 2023, p. 107008. https://doi.org/10.1016/j.icheatmasstransfer.2023.107008

[3] Shaeri, M. R., Bonner, R., and Catuche, J., "Additively Manufactured Hybrid Two-Phase Cold Plate," presented at the ASME 2023 International Technical Conference and Exhibition on Packaging and Integration of Electronic and Photonic Microsystems, San Diego, California, USA, 2023. https://doi.org/10.1115/IPACK2023-109991

[4] Liu, X., Zheng, F., Fu, Q., Song, G., and Xiong, Y., "Thermoelectric Cooler with Embedded Teardrop-Shaped Milli-Channel Heat Sink for Electronics Cooling," *Applied Thermal Engineering*, Vol. 244, 2024, p. 122763. https://doi.org/10.1016/j.applthermaleng.2024.122763

[5] Catuche, J., Shaeri, M. R., and Ellis, M. C., "Additive Manufacturing of Capillary-Driven Two-Phase Cold Plates," Czech Republic, Prague, 2022. https://doi.org/10.11159/htff22.174

[6] Schuderer, J., Bühler, R., and Delincé, F., "Reliability Prediction of a 30 KW Power Electronics Converter," *Microelectronics Reliability*, Vol. 150, 2023, p. 115083. https://doi.org/10.1016/j.microrel.2023.115083

[7] Martinez-Velasco, J. A., and Martin-Arnedo, J., "Power Electronics Applications," *Transient Analysis of Power Systems*, edited by J. Martinez-Velasco, Wiley, 2020, pp. 333–404. https://doi.org/10.1002/9781119480549.ch8

[8] Ren, H., Zou, G., Jia, Q., Deng, Z., Du, C., Wang, W., and Liu, L., "Thermal Stress Reduction Strategy for High-Temperature Power Electronics with Ag Sintering," *Microelectronics Reliability*, Vol. 127, 2021, p. 114379. https://doi.org/10.1016/j.microrel.2021.114379

[9] Zhou, W., Wang, R., Peng, C., and Cai, Z., "Microstructure and Properties of Al–Si Functionally Graded Materials for Electronic Packaging," *Transactions of Nonferrous Metals Society of China*, Vol. 33, No. 12, 2023, pp. 3583–3596. https://doi.org/10.1016/S1003-6326(23)66356-3

[10] Godbole, K., Bhushan, B., Narayana Murty, S. V. S., and Mondal, K., "Al-Si Controlled Expansion Alloys for Electronic Packaging Applications," *Progress in Materials Science*, 2024, p. 101268. https://doi.org/10.1016/j.pmatsci.2024.101268

[11] DeVoto, D., Paret, P., Narumanchi, S., and Mihalic, M., "Reliability of Bonded Interfaces for Automotive Power Electronics," presented at the ASME 2013 International Technical Conference and Exhibition on Packaging and Integration of Electronic and Photonic Microsystems, Burlingame, California, USA, 2013. https://doi.org/10.1115/IPACK2013-73143

[12] Pahinkar, D. G., Boteler, L., Ibitayo, D., Narumanchi, S., Paret, P., DeVoto, D., Major, J., and Graham, S., "Liquid-Cooled Aluminum Silicon Carbide Heat Sinks for Reliable Power Electronics Packages," *Journal of Electronic Packaging*, Vol. 141, No. 4, 2019, p. 041001. https://doi.org/10.1115/1.4043406

[13] Yang, Y., Dorn-Gomba, L., Rodriguez, R., Mak, C., and Emadi, A., "Automotive Power Module Packaging: Current Status and Future Trends," *IEEE Access*, Vol. 8, 2020, pp. 160126–160144. https://doi.org/10.1109/ACCESS.2020.3019775

[14] Shaeri, M. R., Demydovych, M., and Van Pelt, S. C., "CHALLENGES IN FABRICATING CAPILLARY-DRIVEN COLD PLATES USED IN HYBRID TWO-PHASE COOLING SYSTEMS," presented at the 9th Thermal and Fluids Engineering Conference (TFEC), Corvallis, OR, USA, 2024. https://doi.org/10.1615/TFEC2024.elc.050090

[15] Kim, S.-M., and Mudawar, I., "Thermal Design and Operational Limits of Two-Phase Micro-Channel Heat Sinks," *International Journal of Heat and Mass*

Transfer, Vol. 106, 2017, pp. 861–876. https://doi.org/10.1016/j.ijheatmasstransfer.2016.10.020

[16] Dussinger, P., Ju, Y. S., Catton, I., and Kaviany, M., "High Heat Flux, High Power, Low Resistance, Low CTE Two-Phase Thermal Ground Planes for Direct Die Attach Applications," *Ann Arbor*, Vol. 1001, 2012, p. 48109.

[17] Ju, Y. S., Kaviany, M., Nam, Y., Sharratt, S., Hwang, G. S., Catton, I., Fleming, E., and Dussinger, P., "Planar Vapor Chamber with Hybrid Evaporator Wicks for the Thermal Management of High-Heat-Flux and High-Power Optoelectronic Devices," *International Journal of Heat and Mass Transfer*, Vol. 60, 2013, pp. 163–169. https://doi.org/10.1016/j.ijheatmasstransfer.2012.12.058

[18] Shaeri, M. R., Chen, C.-H., Bonner, R. W., and Demydovych, M., "Demonstration of CTE-Matched Two-Phase Minichannel Heat Sink," Orlando, FL, USA, 2023. https://doi.org/10.1109/ITherm55368.2023.10177605

[19] Xu, L., Liu, S., Wang, M., and Zhou, S., "Crack Initiation and Propagation Mechanism of Al2O3-DBC Substrate during Thermal Cycling Test," *Engineering Failure Analysis*, Vol. 116, 2020, p. 104720. https://doi.org/10.1016/j.engfailanal.2020.104720

[20] Xu, L., Wang, M., Zhou, Y., Qian, Z., and Liu, S., "An Optimal Structural Design to Improve the Reliability of Al2O3–DBC Substrates under Thermal Cycling," *Microelectronics Reliability*, Vol. 56, 2016, pp. 101–108. https://doi.org/10.1016/j.microrel.2015.11.013

[21] Sheng, P., Nie, G., Li, Y., Wang, L., Chen, J., Deng, X., and Wu, S., "Enhanced Curing Behavior, Mechanical and Thermal Properties of 3D Printed Aluminum Nitride Ceramics Using a Powder Coating Strategy," *Additive Manufacturing*, Vol. 74, 2023, p. 103732. https://doi.org/10.1016/j.addma.2023.103732

[22] Lin, L., Wu, H., Xu, Y., Lin, K., Zou, W., and Wu, S., "Fabrication of Dense Aluminum Nitride Ceramics via Digital Light Processing-Based Stereolithography," *Materials Chemistry and Physics*, Vol. 249, 2020, p. 122969. https://doi.org/10.1016/j.matchemphys.2020.122969

[23] Xie, Y., Deng, D., Pi, G., Huang, X., and Zhao, C., "Fabrication of Silicon Carbide Microchannels by Thin Diamond Wheel Grinding," *The International Journal of Advanced Manufacturing Technology*, Vol. 111, Nos. 1–2, 2020, pp. 309–323. https://doi.org/10.1007/s00170-020-06085-0

[24] Zhang, B., Li, S., Fei, X., Zhao, H., and Lou, X., "Enhanced Mechanical Properties and Thermal Conductivity of Paraffin Microcapsules Shelled by Hydrophobic-Silicon Carbide Modified Melamine-Formaldehyde Resin," *Colloids and Surfaces A: Physicochemical and Engineering Aspects*, Vol. 603, 2020, p. 125219. https://doi.org/10.1016/j.colsurfa.2020.125219

[25] Chen, Q., Wang, H., Gao, H., Wang, X., and Ma, B., "Effects of Porous Silicon Carbide Supports Prepared from Pyrolyzed Precursors on the Thermal Conductivity and Energy Storage Properties of Paraffin-Based Composite Phase Change Materials," *Journal of Energy Storage*, Vol. 56, 2022, p. 106046. https://doi.org/10.1016/j.est.2022.106046

[26] Bower, C., Ortega, A., Skandakumaran, P., Vaidyanathan, R., and Phillips, T., "Heat Transfer in Water-Cooled Silicon Carbide Milli-Channel Heat Sinks for High Power Electronic Applications," *Journal of Heat Transfer*, Vol. 127, No. 1, 2005, pp. 59–65. https://doi.org/10.1115/1.1852494

[27] Wilson, M. A., Bullough, M., Brooks, K., and Recknagle, K., "Heat and Mass Transfer Design of a Silicon Carbide Micro-Channel Heat Exchanger," presented at the ASME 2003 International Mechanical Engineering Congress and Exposition, Washington, DC, USA, 2003. https://doi.org/10.1115/IMECE2003-55315

[28] Shaeri, M. R., Demydovych, M., and Chen, C.-H., "Additively Manufactured Cold Plate Integrated With Evaporator Wicks and Phase Separators for Thermal Management of Multiple High-Heat-Flux Heat Sources," presented at the ASME 2024 International Technical Conference and Exhibition on Packaging and Integration of Electronic and Photonic Microsystems, San Jose, California, USA, 2024. https://doi.org/10.1115/IPACK2024-141775

[29] Shaeri, M. R., and Demydovych, M., "3D Printed Capillary-Driven Cold Plate for Hybrid Two-Phase Cooling System," presented at the ASME 2024 Heat Transfer Summer Conference collocated with the ASME 2024 Fluids Engineering Division Summer Meeting and the ASME 2024 18th International Conference on Energy Sustainability, Anaheim, California, USA, 2024. https://doi.org/10.1115/HT2024-121704

[30] Shaeri, M. R., and Demydovych, M., "Thermal Management of Multiple High-Heat-Flux Heat Sources Using Additively Manufactured Two-Phase Cold Plate," presented at the 2024 23rd IEEE Intersociety Conference on Thermal and Thermomechanical Phenomena in Electronic Systems (ITherm), Aurora, CO, USA, 2024. https://doi.org/10.1109/ITherm55375.2024.10709620

[31] Shaeri, M. R., and Demydovych, M., "Additively Manufactured Cold Plate with Internal Phase Separator for Hybrid Two-Phase Cooling," presented at the 2024 23rd IEEE Intersociety Conference on Thermal and

Thermomechanical Phenomena in Electronic Systems (ITherm), Aurora, CO, USA, 2024. https://doi.org/10.1109/ITherm55375.2024.10709435

[32] Shaeri, M. R., Bonner, R. W., and Ellis, M. C., "Thin Hybrid Capillary Two-Phase Cooling System," *International Communications in Heat and Mass Transfer*, Vol. 112, 2020, p. 104490. https://doi.org/10.1016/j.icheatmasstransfer.2020.104490

[33] Shaeri, M. R., Attinger, D., and Bonner, R., "Feasibility Study of a Vapor Chamber with a Hydrophobic Evaporator Substrate in High Heat Flux Applications," *International Communications in Heat and Mass Transfer*, Vol. 86, 2017, pp. 199–205. https://doi.org/10.1016/j.icheatmasstransfer.2017.05.028

[34] Shaeri, M. R., Attinger, D., and Bonner, R. W., "Vapor Chambers with Hydrophobic and Biphilic Evaporators in Moderate to High Heat Flux Applications," *Applied Thermal Engineering*, Vol. 130, 2018, pp. 83–92. https://doi.org/10.1016/j.applthermaleng.2017.11.051

[35] Shaeri, M. R., Bonner, R., and Pearlman, H., "ENHANCING HEAT TRANSFER RATES ACROSS DIFFERENT FLOW REGIMES USING PERFORATED-FINNED HEAT SINKS," presented at the Second Thermal and Fluids Engineering Conference, Las Vegas, USA, 2017. https://doi.org/10.1615/TFEC2017.emi.017016